

# Investigating the Freeze-Thaw Damage in Asphalt Concrete Using Imaging Techniques

Mai M. Alawneh  
Ph.D. Candidate  
Department of Civil, Geological and Environmental Engineering  
University of Saskatchewan  
E-mail: [maa592@usask.ca](mailto:maa592@usask.ca)

Haithem Soliman, Ph.D.  
Assistant Professor  
Department of Civil, Geological and Environmental Engineering  
University of Saskatchewan  
E-mail: [Haithem.Soliman@usask.ca](mailto:Haithem.Soliman@usask.ca)

Ania Anthony, M.Sc., P.Eng.  
Director, Materials and Surfacing  
Saskatchewan Ministry of Highways and Infrastructure  
E-mail: [Ania.Anthony@gov.sk.ca](mailto:Ania.Anthony@gov.sk.ca)

This paper was prepared for presentation at the Innovations in Pavement Management, Engineering and Technologies (PS) Session at the **2020 TAC** Conference & Exhibition, online conference.

## Acknowledgements

We would like to acknowledge Al-albayt University/Jordan and the University of Saskatchewan/Canada for funding this research and Canadian Light Source (CLS) for rewarding us beamtimes to scan our samples using X-ray CT scan system.

## Abstract

In cold regions, asphalt concrete (AC) pavements experience freeze-thaw (F-T) cycles that can cause serious damages to AC mixtures. F-T damages in AC mixtures can be related to a cohesion failure within asphalt binders and/or an adhesion failure between coarse aggregate particles and asphalt binder. Accumulation of F-T damages in AC mixtures accelerates the deterioration of pavement structures and reduce their service life and service level. A better understanding of changes in the internal structure of AC mixtures due to F-T cycles paves the way to optimize materials selection and design. In this study, two AC mixtures, without recycled asphalt pavement (RAP) and with 10% RAP, were evaluated before and after 30 F-T cycles using two imaging techniques: digital camera and X-ray computer tomography (CT) scan system. From digital camera images, two types of damage were identified and measured after F-T cycling: breakage within coarse aggregates and adhesion loss between coarse aggregates and fine aggregate matrix (FAM). In addition to breakage of coarse aggregates and adhesion loss, analysis of X-ray CT scan images provided measurements for the change in the width of pre-existing cracks within coarse aggregates due to F-T cycling. The samples will be exposed to addition 30 F-T cycles and evaluated by stereomicroscopic imaging and indirect tension testing (IDT), which were delayed due to the COVID-19 pandemic and will be completed after reopening of labs. The results presented in this paper are part of an ongoing research project. More samples and types of AC mixtures will be tested to evaluate their performance in a F-T cycling environment.

**Key Words:** *asphalt concrete (AC), freeze-thaw (F-T) cycles, indirect tension test (IDT), digital camera, stereomicroscope, X-ray computer tomography (CT) scan, adhesion failure, cohesion failure, broken aggregate, and micro cracks.*

## 1. BACKGROUND

Asphalt concrete (AC) or asphalt mixture is the top layer of the flexible pavement. It is a heterogeneous mixture that consists of aggregates in different sizes, asphalt binder, and air voids. The behaviour of the AC mixture depends highly on its internal structure. After exposure to freeze-thaw (F-T) cycling, the loss of adhesion at the asphalt binder-aggregate interfaces and/or the loss of cohesion within the asphalt binder itself deteriorate the integrity of the AC mixture (Si et al. 2014, Goh and You 2012). **Figure 1** shows an example for failure mechanism of water infiltration into the microcracks/pores of the AC mix combined with F-T cycling.

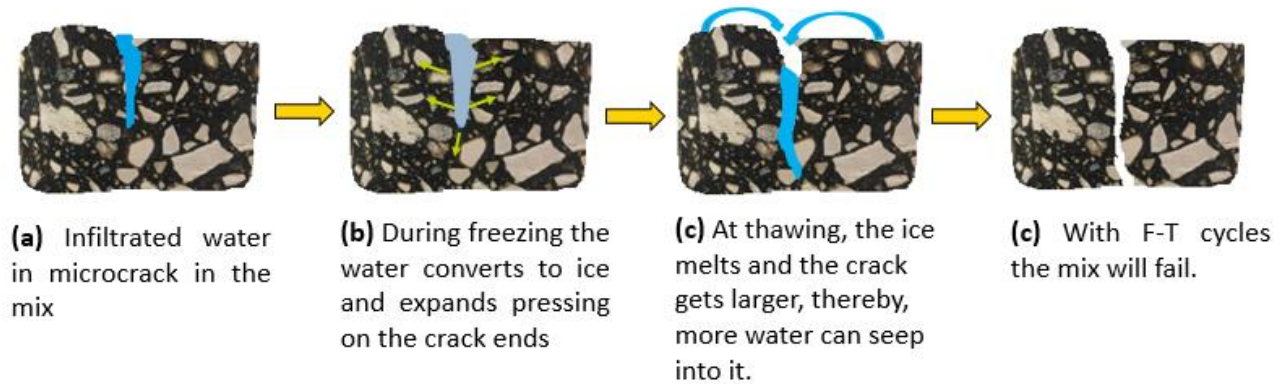


**Figure 1.** F-T response of the infiltrated water inside the AC

Several studies investigated the effect of F-T cycles on the service life of AC pavements using mechanical tests (Guo et al. 2014, Wasiuddin et al. 2014, and Feng et al. 2010). Tarefder et al. (2018) evaluated the effect of F-T cycles on the fatigue life of AC pavement using the Bending Beam Rheometer (BBR) test. Test results showed that the damage in asphalt binders due to F-T cycles resulted in a reduction in the stiffness and fatigue life of AC (Tarefder et al. 2018). Özgan and Serin (2013) investigated the impact of F-T cycles on the performance of AC by exposing asphalt binder specimens to F-T cycles for 24 days. Özgan and Serin (2013) concluded that F-T cycles reduced the Marshall Stability value by 63.8% due to F-T cycles. The F-T response in the previous two studies was investigated at the macro level; while several events affecting this macroscopic response occur at the microscopic level.

Imaging techniques became key tools in characterizing the internal structure of many engineering materials accurately. Imaging techniques were used to analyze the internal structure of AC such as aggregate gradation, aggregates distributions, aggregate orientations, volumetric properties, and 3D reconstruction of the mixture (Masad et al. 1999, Hao et al., 2009, Hamzah et al., 2014, Obaidat et al. 2017). However, limited studies used imaging techniques to assess the impact of the F-T cycles on the internal structure of AC that affects its long-term performance in cold regions.

Hamzah et al. (2014) used a high-resolution optical device and image analysis to assess the adhesion failure due to F-T conditioning on Warm Mix Asphalt (WMA). WMA samples with two different asphalt binders (PG-76 and PG-64) were evaluated after exposure to F-T cycles. The percent of adhesion failure was estimated by evaluated using image analysis techniques after the WMA specimens were tested using the direct tensile strength (DTS) test. It was concluded that the area of adhesion failures increased with the increase in the number of F-T cycles. In addition, samples containing PG-76 binder experienced lower adhesion failures than samples containing PG-64 binder. This may be due to lower freezing temperatures of PG-76 than PG-64 binders. According to findings from this study, imaging techniques can provide a more comprehensive

assessment of adhesion failures in AC when compared to conventional mechanical tests and visual inspection of samples.

X-ray computed tomography (CT) was used for AC damage investigation, which is a non-destructive imaging technique with no sample treatment required before scanning. Using X-ray CT scans, Wang et al. (2003) defined three parameters to characterize the internal structural damage of ACs: air void/crack surfaces, the area between cracks, and average failure size. Khan et al. (2012) used an X-ray CT scan to study the correlation between the change in air void content of AC due to moisture damage and the change in AC stiffness obtained from conventional mechanical testing. Using an X-ray CT scan, Xu et al. (2015, 2018) concluded that the internal structure of AC under F-T events degraded in three ways: existing void expansion, adjacent void merger, and new void formation. Lamothe et al. (2015) used X-ray CT scan and strain gauges to detect the strain distribution on the surface of AC samples during F-T cycles. Lamothe et al. (2015) reported that AC samples partially saturated with water had more changes in volume during F-T cycles than unsaturated AC samples due to the formation and melting of ice inside pores of the AC mixture.

## 2. OBJECTIVES

In this paper, the internal structures of two different samples of AC (without RAP and with 10% RAP) were evaluated before and after 30 F-T cycles. Two imaging techniques were used digital camera imaging, using an iPhone XR cellular phone, and X-ray CT scan in the Biomedical Imaging and Therapy Facility (BMIT) - Insertion Device (ID) beamline at the Canadian Light Source (CLS). 2D images for the internal structure of the samples were collected and analyzed before and after 30 F-T. The changes in the internal structure of these samples were captured and tracked to quantify F-T damage. The samples will be evaluated using stereomicroscopic imaging and Indirect Tension test (IDT), which were delayed due to the COVID-19 pandemic. The results of this study can help municipalities and decision-makers to optimize design and selection of AC materials in a F-T cycling environment.

The main objectives of this study are:

1. Investigate the effect of F-T cycling on different AC mixtures using two different techniques: Mechanical technique which is the Indirect Tension Test (IDT), and imaging technique including digital Camera, stereomicroscope and X-ray CT scan.
2. Quantify the F-T damage in AC according to adhesion failure (%), cohesion failure (%), broken aggregate (%), and the total length of microcracks (mm).
3. Have a better understanding of the F-T damage mechanism in the AC mixes.

### 3. SAMPLES PREPARATION AND CONDITIONING

#### 3.1 AC Samples

AC field cores, 100 mm in diameter and 150 mm in height, were collected from different projects with different types of AC mixtures (0% RAP and 10% RAP). Each sample was cut into two slices (diameter=100 mm and height=38 mm height), and one small core (diameter =50 mm and height =50 mm), as shown in **Figure 2**. Before exposing to F-T cycles, the faces of the slices were mapped using an iPhone XR camera and a Nikon stereomicroscope and the extracted small cores, **Figure 2 (b)**, were scanned at Canadian Light Source (CLS) using x-ray CT system.

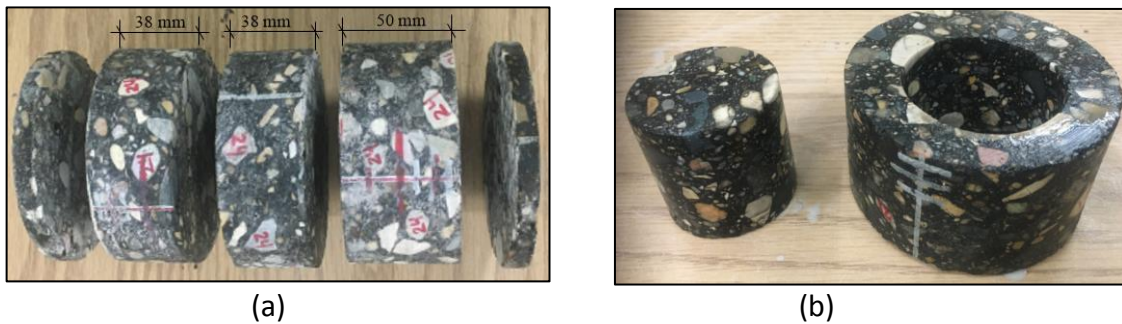


**Figure 2.** AC samples for F-T testing: (a) Cutting samples into slices (b) extracted small core for X-ray CT scan.

#### 3.2 Sample Saturation

Before F-T conditioning, samples were saturated using vacuum saturation to make sure that permeable air voids in the sample are filled with water. A modified method of NCHRP 246 was used in this study. Samples were placed in a desiccator with distilled water covering the samples under pressure ( $P \leq 5 \times 10^{-4}$  torr) for 10 minutes, as shown in **Figure 3**. Then, the vacuum pump was stopped, and the samples were left under a constant low-pressure vacuum. A constant low-pressure vacuum is required to reach a certain percentage of saturation in AC specimens without creating severe micro-damage (Yi et al., 2016). Samples reached full saturation after two weeks.



**Figure 3.** Vacuum saturation of AC Samples

### 3.3 Freeze and Thaw (F-T) Conditioning

After saturation, samples were subjected to 30 F-T cycles using an environmental chamber. The cooling /heating rate of air inside the chamber was  $1.33\text{ }^{\circ}\text{C}/\text{min}$ . The duration of one F-T cycle was 24 hours with 12 hours of freezing at  $-20\text{ }^{\circ}\text{C}$  and 12 hours of thawing at  $+20\text{ }^{\circ}\text{C}$ , as shown in **Figure 4**. These temperatures are the average temperatures in Saskatoon-Canada during winter and summer, respectively, according to the world weather online website from 2009 to 2020, **Figure 5**.

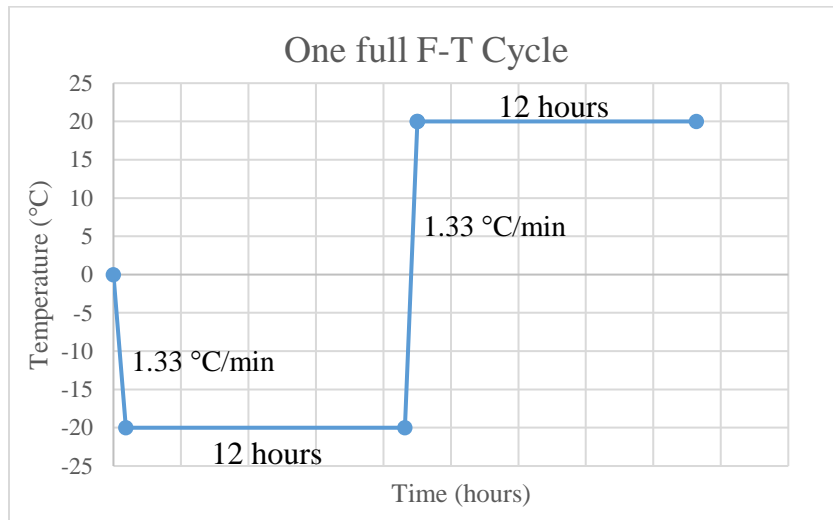


**Figure 4.** One full F-T cycles for 24 hours (one day).

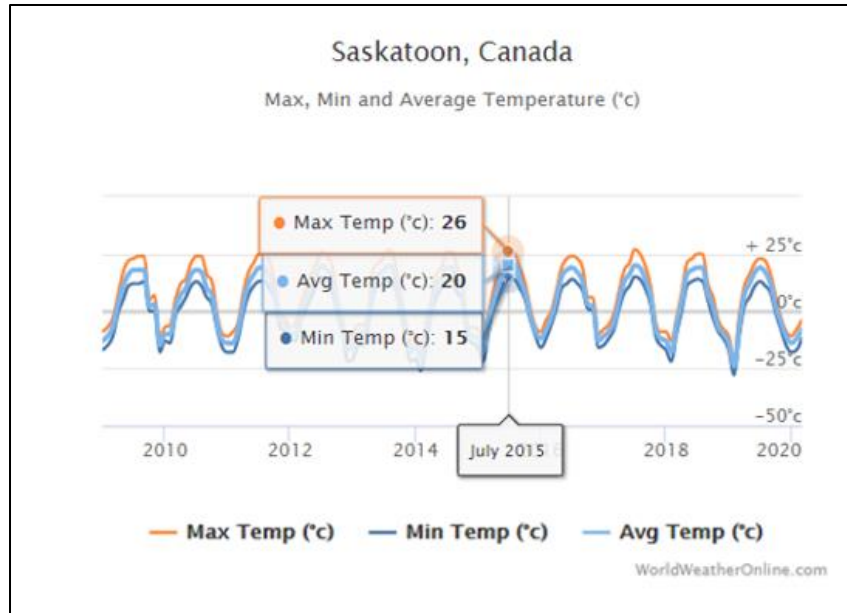


**Figure 5.** Minimum, maximum and average temperatures in Saskatoon-Canada through the years from 2009 to 2019 according to the world weather online website (<https://www.worldweatheronline.com/saskatoon-weather/saskatchewan/ca.aspx>).

#### 4. IMAGING TECHNIQUES

A digital image gives image data of a sample surface as it directly computes the absorption and dispersion characteristics of the area under assessment. An image is a composition of pixels. A pixel is the smallest element in an image, and the number of bits per pixel (bpp) controls how many distinguished colours can be represented by a pixel. Any structural changes of an AC surface in the region of interest in the image are reflected in the matrices representing the image. Based on this basic concept, changes in the internal structure of AC mixtures can be captured from the analysis of digital images (Hamzah et al. (2014)).

Timely imaging assessments are needed with the increasing number of F-T cycles to establish whether damage has happened; if so, it is essential to know where the initiation came through, why the failure is there, and its size. Therefore, the changes in the internal structure such as micro-cracks can be measured from the image analysis.

Image analysis of F-T conditioned samples can help in characterizing the failure mechanism of AC samples. **Figure 6** shows the types of F-T damage that can present in the internal structure of AC mixtures. Broken particles of coarse aggregate indicate that the coarse aggregate matrix in the main source of F-T damage in the AC mixture. Adhesion failure indicates that the bond between

coarse aggregate particles and asphalt binder cannot resist F-T cycling. A cohesion failure within the asphalt binder indicates that the asphalt binder cannot resist F-T cycling.

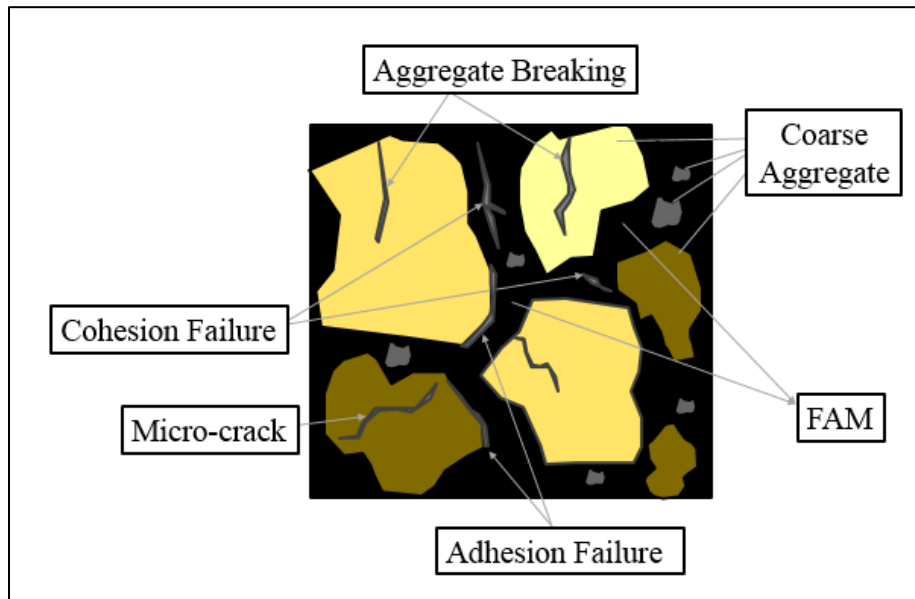


**Figure 6.** Types of F-T damage in AC mixtures

#### 4.1 First Technique: Digital Camera

In this technique, an iPhone XR camera with a resolution of 1.4  $\mu\text{m}$  or 326 pixels per inch (ppi) was used to collect a set of top view 2D images for the AC slices. A tripod was used to fix the phone at a height of 20 cm above the samples. The upper and lower surface of each slice were mapped before F-T cycling and after 30 F-T cycles. **Figure 7** shows the iPhone imaging set-up.

#### 4.2 Second Technique: Stereomicroscopy

The microscopic technique can be employed to provide magnified images that show more details about the internal structure of the AC mixture. Stereomicroscopes are powerful tools in this area as they provide a high level of precision, allowing the micro changes in the AC internal structure to be identified and analyzed under high-resolution. Nikon stereomicroscope (SMZ1270i), **Figure 8**, with high camera resolution (1.32  $\mu\text{m}$ ) and a best-in-class zoom ratio of 12.7x (0.63x-8x), was used to get magnified images for the upper and lower surface of the AC slices. 2D images were collected before F-T cycling for the same surfaces that were mapped using the previous technique. The samples supposed to be evaluated again after 30 F-T cycles, but the test was delayed to the current circumstances related to the coronavirus situation.



**Figure 7.** Digital camera imaging set-up.



**Figure 8.** Stereomicroscope (SMZ1270i) with AC slice.

### 4.3 Third Technique: X-ray CT Scan

The small cores that were extracted from the AC field samples were scanned using the X-ray CT system at the Canadian Light Source (CLS). The small cores, 50 mm in diameter and 50 mm in height, were scanned using the Biomedical Imaging and Therapy Facility (BMIT) - Insertion Device (ID) beamline, **Figure 9**. A core size of 50mm x 50mm is the maximum size that can be scanned at the BMIT-ID beamline in CLS with a high resolution of 13  $\mu\text{m}$ .

The BMIT-ID beamline delivers an X-ray beam with a photon flux density enough to acquire a monochromatic CT scans in a relatively short time. The spectral range extends to 140 keV, which can be used to penetrate through thick and absorbing samples, such as AC cores, and investigate their internal structure. **Table 1** shows a comparison between the imaging techniques used in this study.



**Figure 9.** BMIT-ID beamline at CLS

**Table1.** Comparison between the imaging techniques used in this study.

<b>Imaging Technique</b>	<b>iPhone camera imaging</b>	<b>Stereomicroscope imaging</b>	<b>X-ray CT Scan</b>
<b>Sample Size</b>	Slice (d= 100 and h= 38mm)	Slice (d= 100 and h= 38mm)	Small core (d= 50mm and h= 50mm)
<b>Sample Penetration</b>	Cannot penetrate the sample surface	Cannot penetrate the sample surface	Can penetrate the sample and reveal all details of the internal structure
<b>Type of Produced images</b>	2D images for the cross-section surface	Magnified 2D images for the cross-section surface	2D cross-sections and 3D reconstruction for the entire sample
<b>Source</b>	Light	Light	X-ray beam (Photon current)
<b>Imaging Tools</b>	iPhone XR camera Tripod Computer Image processing software	Stereomicroscope Computer Image processing software	X-ray CT scan machine Sample holder Computer Image processing software
<b>Image Resolution</b>	1.4 microns	1.32 microns	13 microns

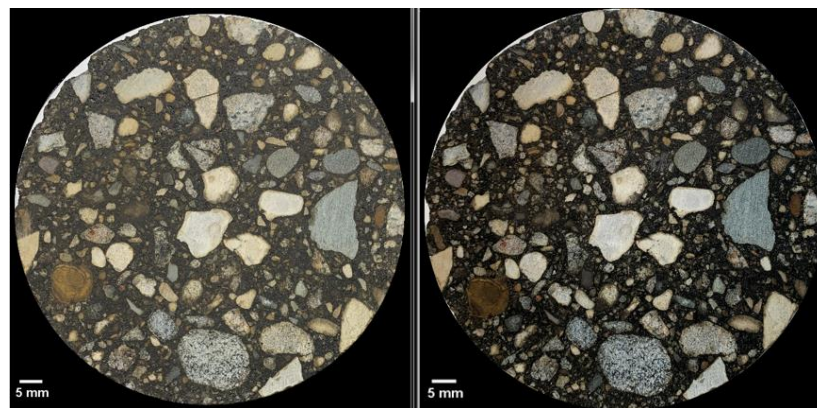
## 5. IMAGE ANALYSIS

The initial results presented in this paper are part of the calibration and validate the procedure for the research methodology. **Table 2** shows the testing matrix in this paper. Two types of mixtures were investigated before and after 30 F-T cycles. These mixtures are a typical AC mixture will all virgin materials and a typical AC mixture with 10% of recycled asphalt pavement (RAP). One slice from each mixture was used for 2D imaging using a digital camera, and one small core was used for the X-ray CT scan.

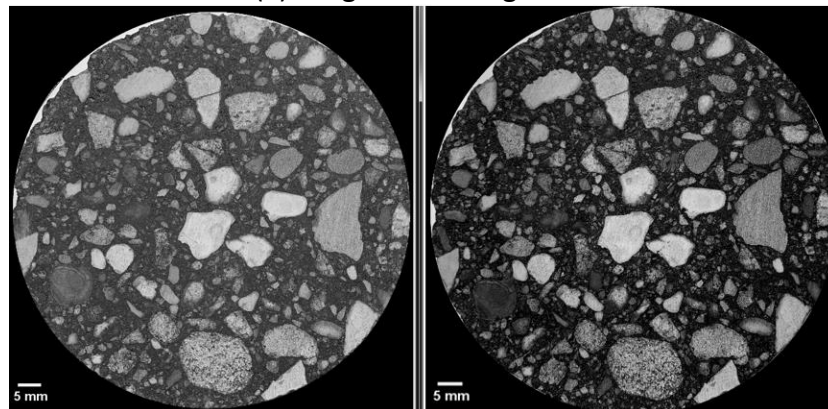
**Table 2:** Testing Matrix

<b>Type of mix</b>	<b>No. of Samples</b>	<b>Dimensions</b>	<b>Type of Testing</b>
Typical (0 RAP%)	1	d= 50mm and h= 50mm	X-ray CT scan
	2	d= 100 and h= 38mm	iPhone imaging
Typical with 10 RAP%	RAP-1	d= 50mm and h= 50mm	X-ray CT scan
	RAP-2	d= 100 and h= 38mm	iPhone imaging

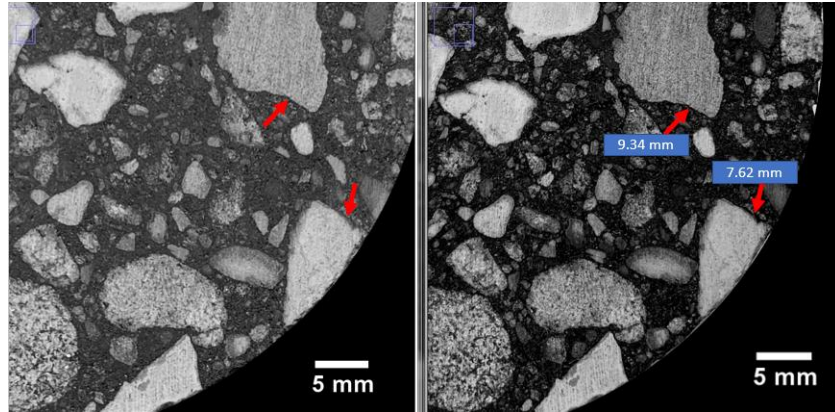
ImageJ software was used to analyze the collected 2D images and CT scans. ImageJ is a public domain Java image processing program. The software can measure distances, areas, and angles. In addition, ImageJ supports standard image processing functions such as contrast manipulation, sharpening, smoothing, edge detection, and median filtering. All analysis and processing functions are available at any magnification factor. This software is used extensively for biological tasks such as cell detection, but it was used in this study for microanalysis of AC mixtures. **Figure 10(a)** shows the images taken by the digital camera for the lower face of sample 2 (0% RAP) before and after 30 F-T cycles. To be analyzed using ImageJ, the coloured images were converted to 8-bit images, as shown in **Figure 10(b)**. **Figure 10(c)** shows that after 30 F-T cycles, there is a loss of adhesion between the coarse aggregates and the fine aggregate matrix (FAM). **Figure 10(d)** shows a broken coarse aggregate particle and more adhesion loss within the mixture. The total length of the micro-cracks in this cross-section was 28.79 mm.



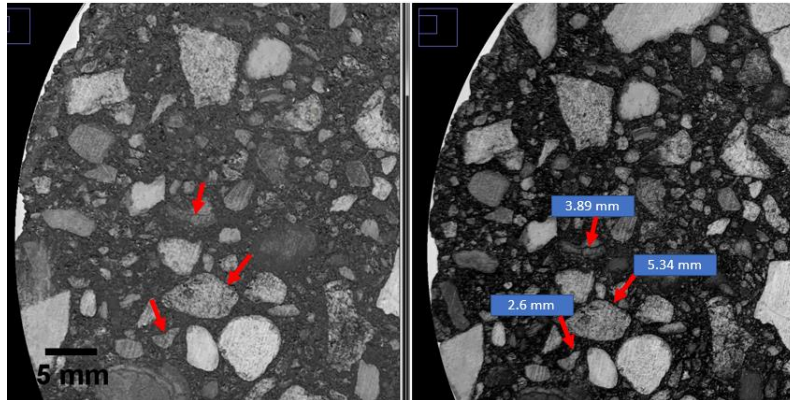
(a) Original 2D images



(b) 8-bit images



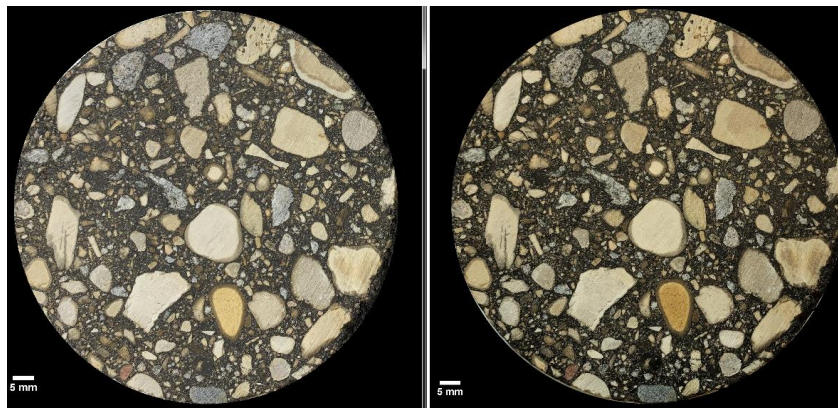
(c) Adhesion failures at lower-left part of the sample



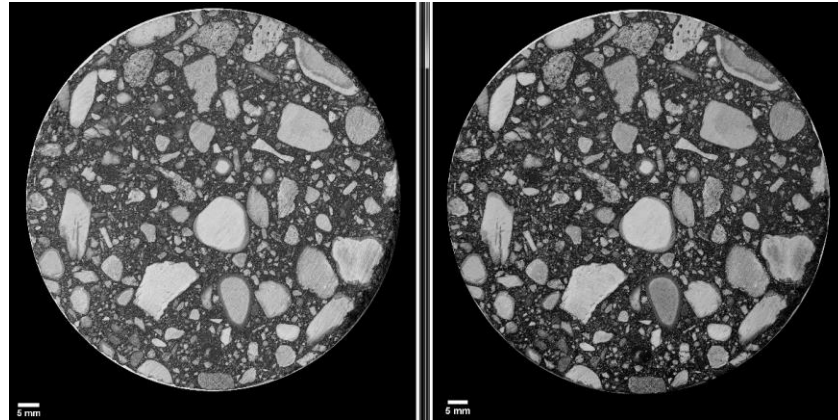
(d) Broken aggregate and adhesion failures at the left side of the sample

**Figure 10.** ImageJ analysis for 2D digital camera images of the lower face of sample 2 (0% RAP) at 0 F-T cycles (right) and after 30 F-T cycles (Left)

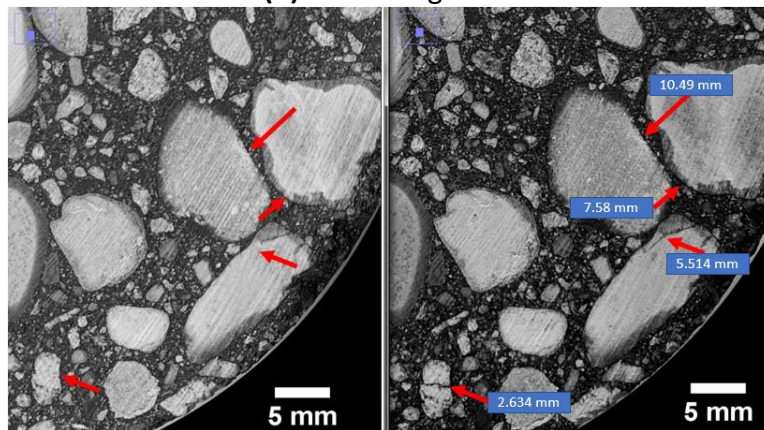
**Figure 11(a)** shows the images taken by the digital camera for the lower face of sample RAP-2 (10% RAP) before and after 30 F-T cycles. After 30 F-T cycles, sample 4 experienced length increase of exiting micro-crack in coarse aggregates, breakage of coarse aggregates, and adhesion loss between coarse aggregates and FAM as shown in **Figures 11(c)** and **11(d)**. The total length of the micro-cracks in this cross-section was 27.43 mm.



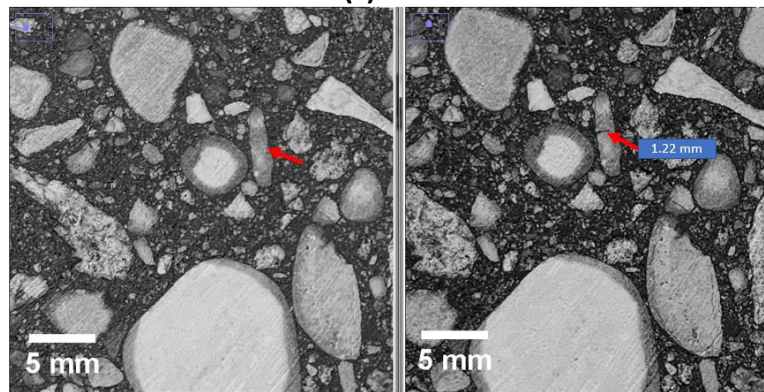
(a) Original 2D images



(b) 8-bit images



(c)

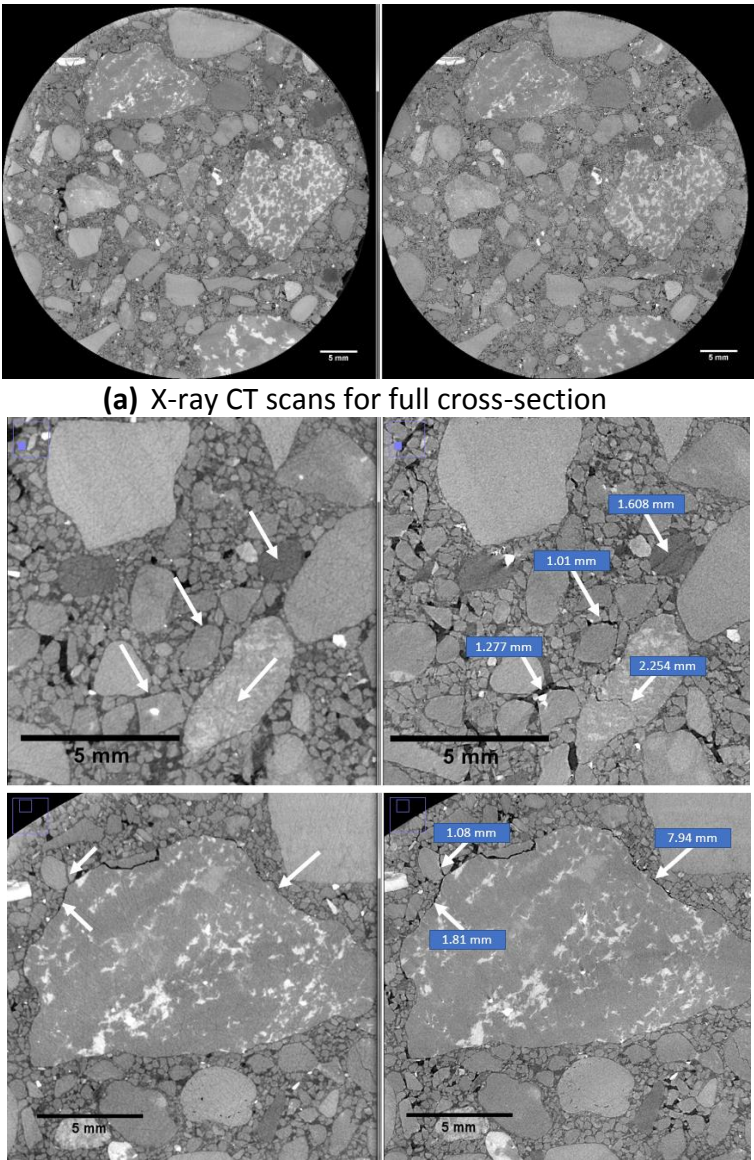


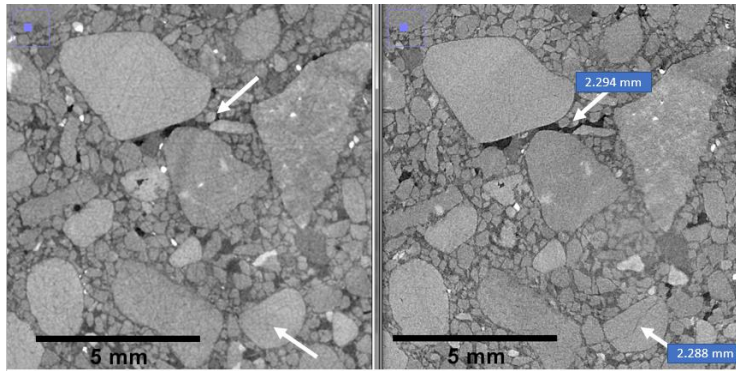
(d)

**Figure 11.** ImageJ analysis for 2D digital camera images of the lower face of sample RAP-2 (10% RAP) at 0 F-T cycles (right) and after 30 F-T cycles (Left).

The results from the analysis of digital camera images showed that the two dominant types of damage after 30 F-T cycles are breakage of coarse aggregates and adhesion loss between coarse aggregates and FAM. In addition, pre-existing micro-cracks in coarse aggregates experienced an increase in length after F-T cycling. The total length of micro-cracks in sample RAP-2 with 10% RAP was lower than that in sample 2 with 0% RAP. However, the difference in micro-cracks length between the two samples was not significant.

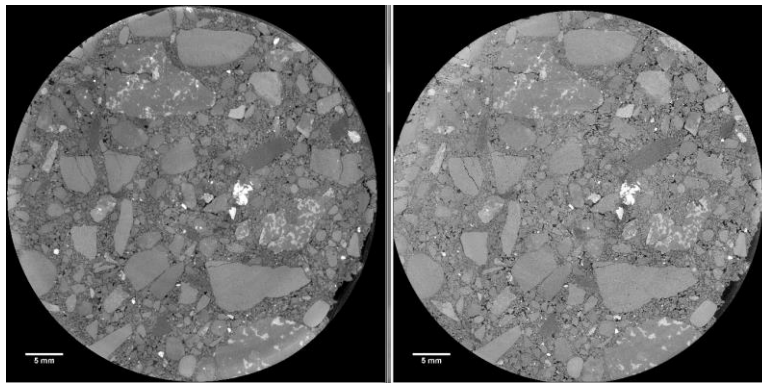
A cross-section from the X-ray CT scan for sample 1 core (0% RAP) was analyzed using ImageJ software. The X-ray CT scans for the cross-section before and after 30 F-T cycles are shown in **Figure 12(a)**. **Figure 12(b)** shows examples of observed breakage in coarse aggregates and adhesion loss between coarse aggregates and FAM. The total length of micro-cracks in this cross-section was 29.75 mm. **Figures 13(a)** and **13(b)** show X-ray CT scans for the same sample, sample 1, but for a second cross-section at a different height of the sample. From **Figure 13**, the observed damage types in the second cross-section were also breakage of coarse aggregates and adhesion loss between coarse aggregates and FAM. Also, the width of pre-existing cracks in coarse aggregates increased after F-T cycling, as shown in **Figure 13(b)**. The total length of micro-cracks in the second cross-section was 24.94 mm.



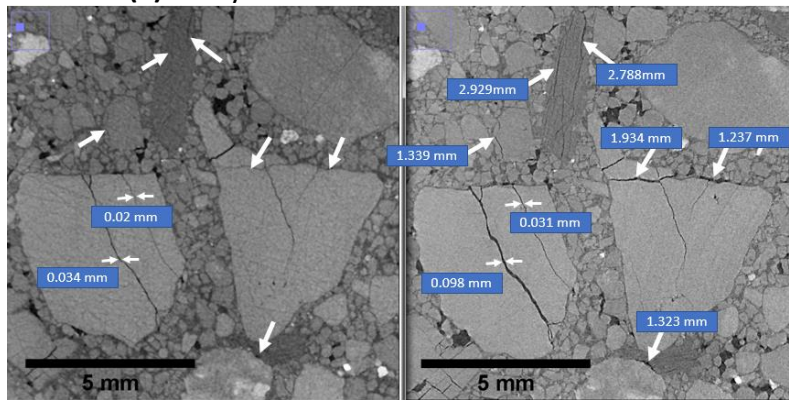


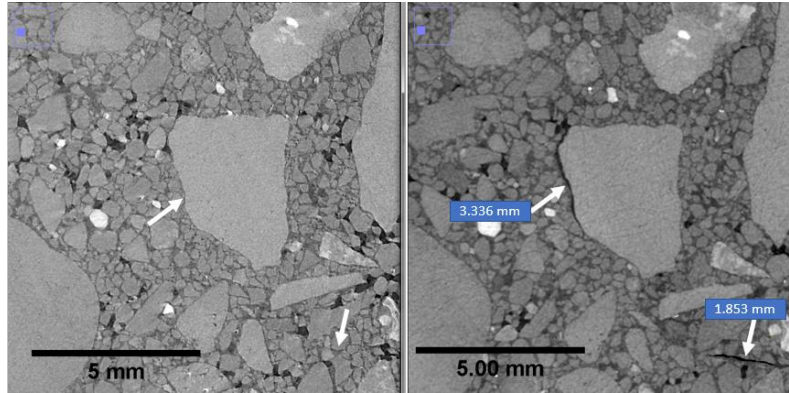
**(b)** Broken coarse aggregates and adhesion failures

**Figure 12.** ImageJ analysis for X-ray CT scans of sample 1 (0% RAP) at 0 F-T cycles (right) and after 30 F-T cycles (Left) – cross-section 1



**(a)** X-ray CT scans for full cross-section

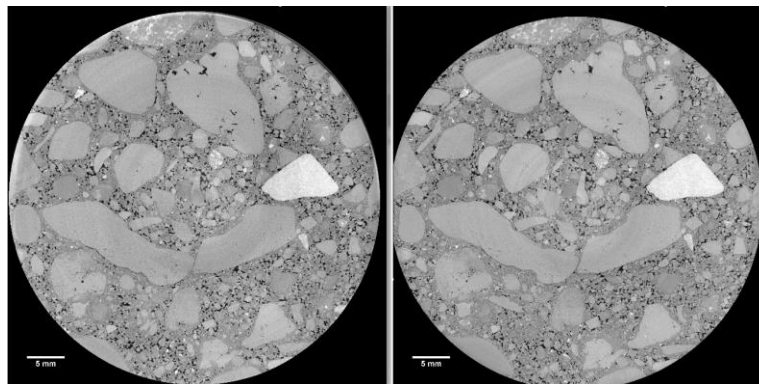




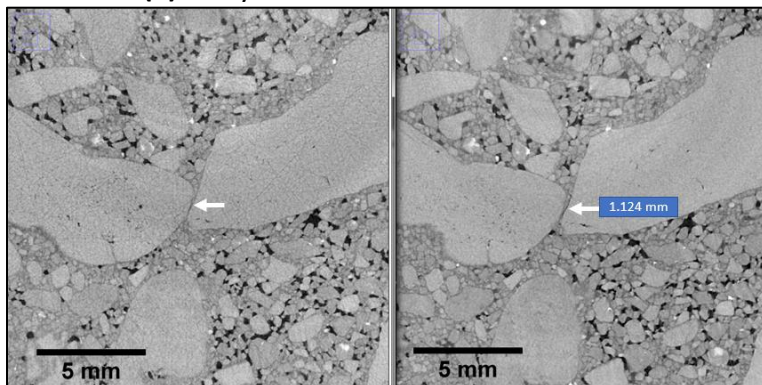
(b)

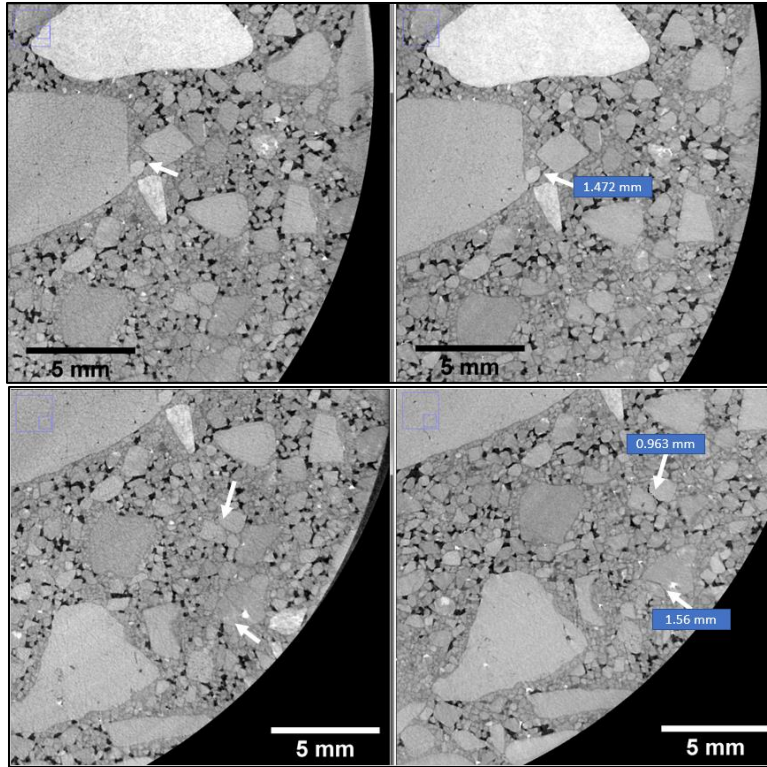
**Figure 13.** ImageJ analysis for X-ray CT scans of sample 1 (0% RAP) at 0 F-T cycles (right) and after 30 F-T cycles (Left) – cross-section 2

Using the same procedures for sample 1, two X-ray CT scan cross-sections at different depths were analyzed for sample RAP-1 (10% RAP). **Figures 14** and **15** show the X-ray scans for the first and second cross-sections, respectively, before and after 30 F-T cycles. Similar to sample 1, the dominant damage types after F-T cycling were breakage of coarse aggregates, adhesion loss between coarse aggregates and FAM, and increase in width of pre-existing cracks in coarse aggregates. For the first cross-section, the total length of micro-cracks was 5.12 mm. For the second cross-section, the total length of micro-cracks was 5.00 mm.



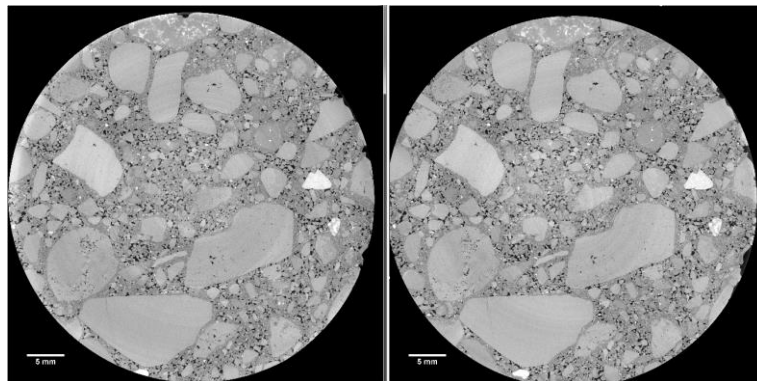
(a) X-ray CT scans for full cross-section



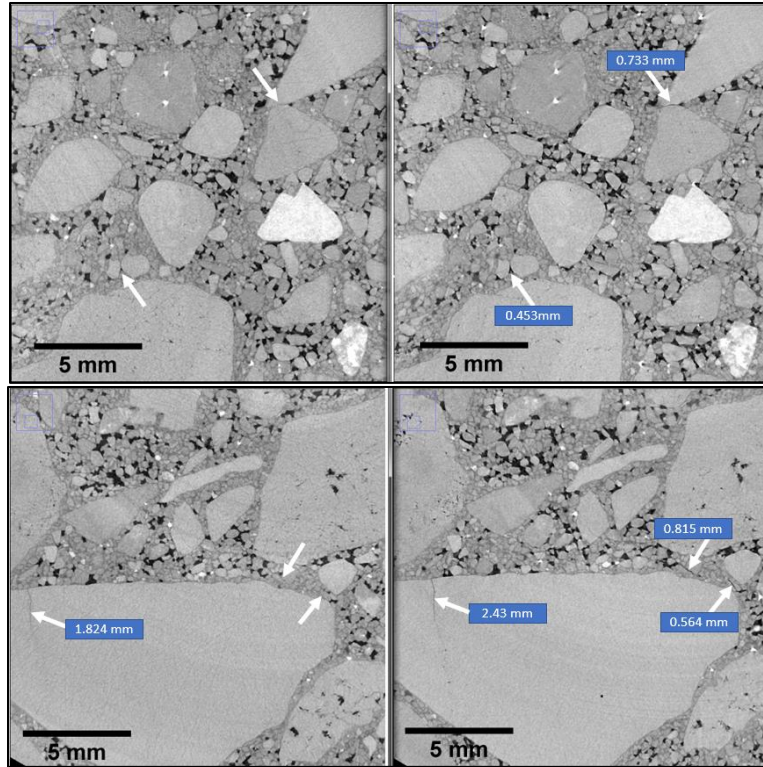


(b) Broken coarse aggregates and adhesion failures

Figure 14. ImageJ analysis for X-ray CT scans of sample RAP-1 (10% RAP) at 0 F-T cycles (right) and after 30 F-T cycles (Left) – cross-section 1



(a) X-ray CT scans for full cross-section



(b) Broken coarse aggregates and adhesion failures

**Figure 15.** ImageJ analysis for X-ray CT scans of sample RAP-1 (10% RAP) at 0 F-T cycles (right) and after 30 F-T cycles (Left) – cross-section 2

The results from the analysis of X-ray CT scan images showed that the three dominant types of damage after F-T cycling are breakage of coarse aggregates, adhesion loss between FAM and coarse aggregates, and increase in width of pre-existing cracks in aggregates. For the particular samples and cross-sections analyzed in this paper, the total length of micro-cracks in the 10% RAP sample was lower than that in the 0% RAP sample by approximately 81%. **Table 3** shows a summary of the image analysis results.

**Table 3.** Summary of the image analysis results

RAP %	Sample ID.	Sample size	Type of testing	Assessed part	Micro-crack length (mm)
0 RAP%	1	Small core (d= 50mm and h= 50mm)	X-ray CT scan	Cross-section 1	29.75
				Cross-section 2	24.94
	2	Slice (d= 100 and h= 38mm)	iPhone imaging	Lower face	28.79
10 RAP%	RAP-1	Small core (d= 50mm and h= 50mm)	X-ray CT scan	Cross-section 1	5.12
				Cross-section 2	5.00
	RAP-2	Slice (d= 100 and h= 38mm)	iPhone imaging	Lower face	27.43

## 6. SUMMARY

AC is a composite material of mineral aggregate, asphalt binder and air voids. During wet weather conditions, water infiltrates into the micro-cracks and permeable pores of AC mixtures. In freezing weather conditions, the infiltrated water becomes ice crystals and increase in volume, which produces an internal pressure on the components of AC mixtures. With repeated cycles of freezing and thawing, AC mixtures can experience internal damages and deterioration.

This study investigates internal changes within AC mixtures after exposure to F-T cycling using imaging techniques. Two types of mixtures, with no RAP and with 10% RAP, were tested before and after 30 F-T cycles. Two imaging techniques were used: digital camera and X-ray CT scan. From the analysis of digital camera images, two types of damage were identified and measured after F-T cycling: breakage within coarse aggregates and adhesion loss between coarse aggregates and FAM. In addition to breakage of coarse aggregates and adhesion loss, analysis of X-ray CT scan images provided measurements for the change in the width of pre-existing cracks within coarse aggregates due to F-T cycling.

The samples will be exposed to additional 30 F-T cycles and evaluated again by imaging techniques and indirect tension testing (IDT). The stereomicroscopic imaging and indirect tension (IDT) tests were delayed due to the COVID-19 pandemic and will be completed after the reopening of labs. The stereomicroscope images will be collected for the same two samples after 30 and 60 F-T cycles and will be compared to the original images at 0 f-T to find out the changes due to F-T cycling. This technique will validate the results from the other imaging technique used in this paper. The IDT will be conducted at 0, 30 and 60 F-T cycles and the results will be correlated to the image analysis results. This paper is a part of an ongoing research project. More samples and different types of AC mixtures will be tested to evaluate their performance in the F-T cycling environment.

## REFERENCES

- Feng, D., Yi, J., Wang, D., & Chen, L. (2010). Impact of salt and freeze-thaw cycles on performance of asphalt mixtures in coastal frozen region of China. *Cold Regions Science and Technology*, 62(1), 34-41.
- Goh, S. W., and You, Z. (2012). "Evaluation of hot-mix asphalt distress under rapid freeze-thaw cycles using image processing technique." *CICTP 2012: Multimodal transportation systems—Convenient, safe, cost-effective, efficient*, ASCE, Reston, VA, 3305–3315.

Guo, N., You, Z., Zhao, Y., Tan, Y., & Diab, A. (2014). Laboratory performance of warm mix asphalt containing recycled asphalt mixtures. *Construction and Building Materials*, 64, 141-149.

Lamothe, S., Perraton, D., and Di Benedetto, H. (2015). "Contraction and expansion of partially saturated hot mix asphalt samples exposed to freeze-thaw cycles." *Road Mater. Pavement Des.* 16(2), 277–299.

Masad, E., B. Muhunthan, N. Shashidhar, and T. Harman. (1999). "Internal Structure Characterization of Asphalt Concrete Using Image Analysis". *Journal of computing in civil engineering*. 13 (2): 88-95.

M.O. Hamzah, M.R. Kakar, S.A. Quadri, J. Valentin, (2014). Quantification of moisture sensitivity of warm mix asphalt using image analysis technique, *J. Cleaner Prod.* 68 200–208.

Obaidat M., Abo-Qudais S., O. A. (2005). Evaluation of Stripping in Bituminous Mixtures Using Conventional and Image Processing Techniques, 33(6), 418–432.

Obaidat, Mohammed T., Khalid A. Ghuzlan, and Mai M. Alawneh. (2017). "Analysis of Volumetric Properties of Bituminous Mixtures Using Cellular Phones and Image Processing Techniques". *Canadian Journal of Civil Engineering*. 44 (9): 715–726.

Özgan, E., & Serin, S. (2013). Investigation of certain engineering characteristics of asphalt concrete exposed to freeze-thaw cycles. *Cold Regions Science and Technology*, 85, 131- 136.

R. Khan, A.C. Collop, G.D. Airey, A.N. Khan, (2012). Asphalt damage characterization from cyclic test and X-ray computed tomography, *Transport* 166 203–213.

Si, W., Ma, B., Li, N., Ren, J. P., and Wang, H. N. (2014). "Reliability-based assessment of deteriorating performance to asphalt pavement under freeze-thaw cycles in cold regions." *Constr. Build. Mater.*, 68, 572–579.

Tarefder, R., Faisal, H., & Barlas, G. (2018). Freeze-thaw effects on fatigue LIFE of hot mix asphalt and creep stiffness of asphalt binder. *Cold Regions Science and Technology*.

Wang, L.B., J.D. Frost, G.Z Voyiadjis, and T.P. Harman. (2003). Quantification of damage parameters using X-ray tomography images. *Mechanics of Materials*. 35 (8): 777-790.

Wasiuddin, N. M., Wilson, K., Islam, M. R., Parker, P., Abadie, C., & Mohammad, L. N. (2014). Field and laboratory evaluation of environmental effects on chip seal performance: Freeze-thaw and asphalt aging. *Journal of Testing and Evaluation*, 43(4), 820-832.

Xu H., Li H., Tan Y., Wang L., and Hou Y. (2018). A micro-scale investigation on the behaviors of asphalt mixtures under freeze-thaw cycles using entropy theory and a computerized tomography scanning technique. *Entropy*. 20 (2): 68.

Xu, H.N.; Guo, W.; Tan, Y.Q. (2015). Internal Structure Evolution of Asphalt Mixtures during Freeze-Thaw Cycles. *Mater. Des*, 86, 436–446.

Y. Hao, Y. Hai-Wen, L. Yuan-Quan, Z. Hai-Xia, Z. Lei, (2009). Air voids measurement on asphalt mixes section surface based on image analysis, In *Electronic Measurement & Instruments, ICEMI'09, 9th International Conference on*, pp. 4–296, IEEE.

Yi, J., Shen, S., Wang, D., Feng, D., Huang, Y., (2016). Effect of Testing Conditions on Laboratory Moisture Test for Asphalt Mixtures. *Journal of Testing and Evaluation*, 44(2), pp.856-867.